Received: 1 October 2018 | Revised: 27 October 2018 | Accepted: 29 October 2018

DOI: 10.1002/hc.21456

RESEARCH ARTICLE

WILEY

Heteroatom Chemistry

Synthesis and properties of redox-switchable zinc complexes of 10,15,20-triaryl-15-aza-5-oxaporphyrin

Keisuke Sudoh[1] | **Ko Furukawa**[2] | **Haruyuki Nakano**[3] | **Soji Shimizu**[4] | **Yoshihiro Matano**[5]

[1]Department of Fundamental Sciences, Graduate School of Science and Technology, Niigata University, Niigata, Japan

[2]Center for Coordination of Research Facilities, Institute for Research Promotion, Niigata University, Niigata, Japan

[3]Department of Chemistry, Graduate School of Science, Kyushu University, Fukuoka, Japan

[4]Department of Chemistry and Biochemistry, Graduate School of Engineering, Kyushu University, Fukuoka, Japan

[5]Department of Chemistry, Faculty of Science, Niigata University, Niigata, Japan

Correspondence
Yoshihiro Matano, Department of Chemistry, Faculty of Science, Niigata University, Niigata, Japan.
Email: matano@chem.sc.niigata-u.ac.jp

Funding information
Japan Society for the Promotion of Science, Grant/Award Number: 18H01961, 15K05392, 18K05036

Abstract

The synthesis, aromaticity, and optical and electrochemical properties of zinc(II) complexes of 10,15,20-triaryl-15-aza-5-oxaporphyrin (TriAAOP) were investigated. Metal-templated cyclization of a zinc(II) 1,19-dichloro-5,10,15-triaryl-10-azatetrapyrrin complex with an oxygen source afforded 20π TriAAOP in the neutral form. Oxidation of 20π TriAAOP with silver (I) hexafluorophosphate generated the 19π radical cation or 18π dication depending on the content of oxidant used. The interconversion between the three oxidation states (18π, 19π, and 20π) resulted in distinct changes in the aromaticity and optical properties of the 15-aza-5-oxaporphyrin π-system. Nuclear magnetic resonance spectroscopy of 20π TriAAOP revealed its antiaromatic character, whereas that of the 18π TriAAOP dication showed its aromatic character. The combined effect of the two *meso*-heteroatoms was directly reflected in the redox properties of the porphyrin ring; TriAAOP was reduced more easily and more difficult to oxidize than the zinc(II) complex of 5,10,15,20-tetraaryl-5,15-diaz-aporphyrin (TADAP). In the ultraviolet-visible-near–infrared spectra of the materials, the lowest-energy electronic excitations of the 19π and 18π TriAAOP derivatives were considerably red-shifted compared with those of the isoelectronic TADAP derivatives. Based on the results of density functional theory calculations, it was concluded that the observed differences between TriAAOP and TADAP would arise from the high electronegativity of oxygen; specific frontier orbitals of the TriAAOP π-systems were energetically stabilized relative to those of the TADAP π-system. The present findings corroborate that the *meso*-modification of a porphyrin rings with different kinds of heteroatoms is a promising strategy to fine tune their light-response properties that are switchable by reversible single electron transfer processes.

A tribute to Professor Naomichi Furukawa on the Occasion of his 82nd birthday - By Invitation only

Contract grant sponsor: JSPS KAKENHI

Contract grant number: 18H01961

Contract grant number: 15K05392

Contract grant number: 18K05036

1 | INTRODUCTION

Porphyrins are well known as redox-switchable macrocycles with optical and electrochemical properties that vary widely depending on the peripheral substituents and/or central metal. In general, two-electron- and one-electron-reduced porphyrins (20π and 19π porphyrins, respectively) are extremely unstable under atmospheric conditions because of their high-energy highest occupied molecular orbital (HOMO) and singly occupied molecular orbital (SOMO), respectively.[1] Several approaches have been proposed to isolate 20π and 19π porphyrins in neutral forms, which basically rely on the concept of lowering the HOMO or SOMO energy levels.[2–22] However, most of the reported neutral 20π and 19π porphyrins are highly distorted and/or still air-sensitive. Little information about the aromaticity and optical properties accompanying redox conversion of the π-systems of neutral 20π and 19π porphyrins is available. It is therefore important to establish a reliable approach to provide reduced forms of porphyrins with flat π-planes and air stability.

Recently, we reported a new approach to synthesize neutral 20π and 19π porphyrins by replacing *meso*-methine units of a porphyrin ring with nitrene units, which was based on the concept of macrocyclic π-conjugation involving the unshared electrons in the p-orbitals of *meso*-nitrogen atoms.[23–25] As expected, 20π and 19π derivatives of 5,10,15,20-tetraaryl-5,15-diazaporphyrin (TADAP)[23,24] and 5,10,20-triaryl-5,15-diazaporphyrin (TriADAP)[25] were isolated in the neutral or cationic form. Most importantly, these novel diazaporphyrin derivatives have very flat π-planes and are extremely air-stable compared with the isoelectronic 20π porphyrin dianions and 19π porphyrin radical anions. Furthermore, the oxidation states of TADAP and TriADAP are switchable through reversible redox processes (Scheme 1), which enabled us to investigate the correlation between the oxidation state and optical and magnetic properties of the porphyrin π-circuit in detail.

In addition to diazaporphyrin derivatives, 20π porphyrins modified with chalcogen atoms at the 5 and 15 positions have received considerable attention from both porphyrin and heteroatom chemists.[26–30] Recently, Shimizu et al.[28] and Shinokubo et al.[29,30] independently reported the nickel(II) complex of 10,20-diaryl-5,15-dioxaporphyrin (DOP) and several metal complexes and the free base of 10,20-diaryl-5,15-dithiaporphyrin (DTP), respectively (Chart 1). It is worth noting that the structure and aromaticity of these heteroporphyrins varied markedly depending on the *meso*-chalcogen atoms. The DOP ring was flat and exhibited 20π antiaromatic character, whereas the DTP rings (M = Ni, Zn) showed considerable bending at the two sulfur atoms and exhibited nonaromatic character. Interestingly, electrochemical oxidation of the 20π DOP did not give the expected 18π dication but its dimer and oligomers via a 19π radical

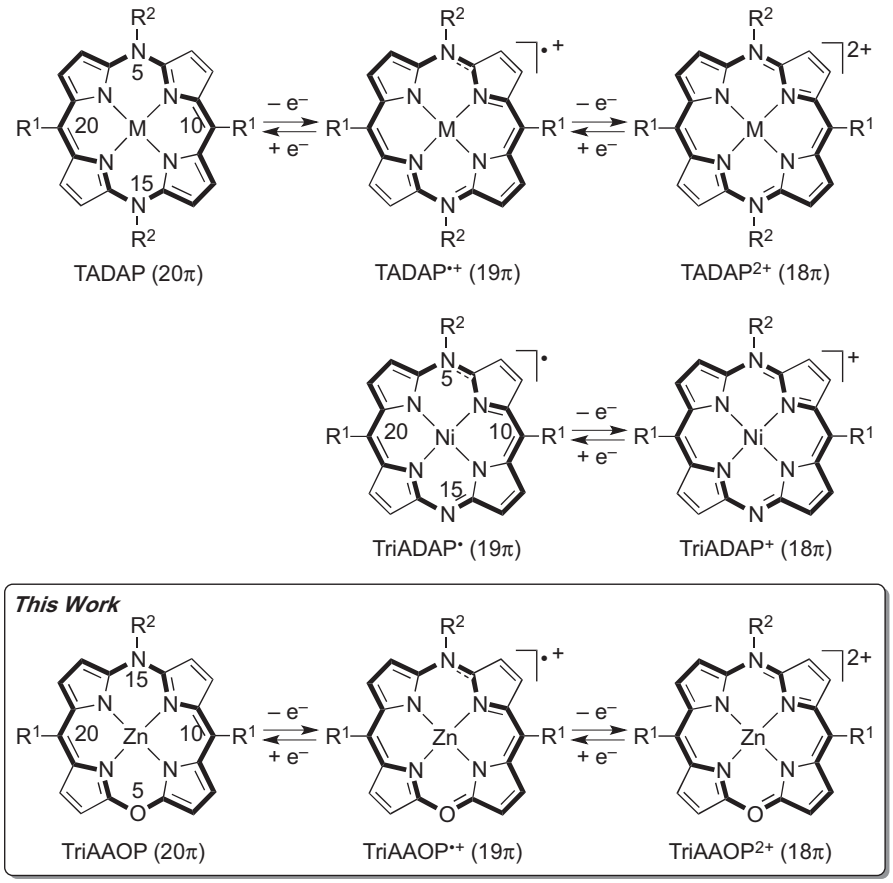

SCHEME 1 Redox reactions of TADAP, TriADAP, and TriAAOP

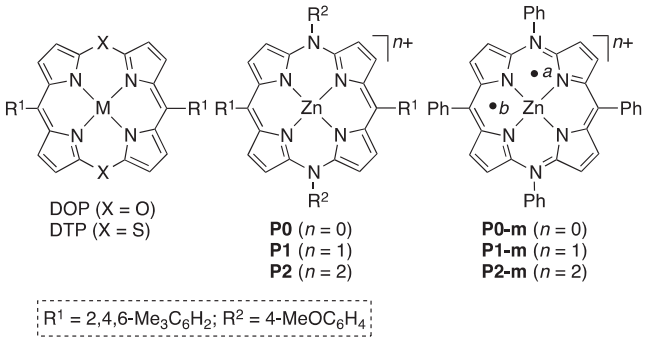

CHART 1 DOP, DTP, TADAPs (**P0**, **P1**, **P2**), and models (**P0-m**, **P1-m**, **P2-m**)

cation intermediate. With these results in mind, we decided to investigate the cooperative effect of an oxygen atom and nitrene unit placed at the 5 and 15 positions, respectively, on the fundamental properties of a porphyrin ring. Herein, we report the first examples of redox-switchable zinc(II) complexes of 10,15,20-triaryl-15-aza-5-oxaporphyrin (TriAAOP, Scheme 1) and discuss their aromatic character and optical properties determined from experimental and theoretical analyses.

2 | RESULTS AND DISCUSSION

2.1 | Synthesis

Scheme 2 illustrates the synthesis of TriAAOP. Treatment of zinc(II) acetate with a mixture of equimolar amounts of 1,9-dichloro-5-mesityldipyrrin **1** (mesityl = 2,4,6-trimethylphenyl)[31] and 1-chloro-9-(4-methoxyphenylamino)-5-mesityldipyrrin **2**[23,24] in the presence of excess triethylamine in CH_2Cl_2/MeOH at room temperature afforded three kinds of zinc(II)–bis(dipyrrin) complexes, **3**, **4**, and **5**, which were successfully separated from one another by column chromatography on silica gel. The unsymmetrically substituted zinc complex **3** was isolated as a reddish brown solid, and the symmetrically substituted zinc complexes **4** and **5** were isolated as reddish brown and orange solids, respectively. Heating a mixture of **3** and potassium carbonate in *N*,*N*-dimethylformamide (DMF) at 110°C for 1 hour afforded the zinc(II) complex of 1,19-dichloro-5,15-dimesityl-10-(4-methoxyphenyl)-10-azatetrapyrrin **6** as a green solid in quantitative yield.

Attempts to synthesize the target compound TriAAOP by sequential S_N2 reactions of **6** with several oxygen sources (Me_4NOH, KOH, Ag_2O) under various conditions were unsuccessful. However, we eventually found that the ring-closure reaction of **6** with excess 4-methoxybenzaldoxime/NaH, which had been used to synthesize DOP,[28] afforded 20π TriAAOP **7** as a yellow solid. Treatment of **7** with silver(I) hexafluorophosphate in CH_2Cl_2 instantaneously generated 19π radical cation **8** or 18π dication **9** depending on the content of oxidant used. The quantitative formation of **8** and **9** in solution was confirmed by ultraviolet-visible-near–infrared (UV-vis-NIR) absorption spectroscopy (vide infra). However, it was difficult to isolate the solid samples of **8** and **9** with high purity because they gradually decomposed in concentrated solutions under atmospheric conditions. This behavior of **8** and **9** was in sharp contrast to the remarkable stability observed for the corresponding TADAP derivatives **P1** and **P2**, although the reason for this difference is not yet clear.

Compounds **7**, **8**, and **9** were characterized by high-resolution electrospray ionization (ESI) mass spectrometry and ^{1}H NMR spectroscopy (for **7** and **9**). In the ESI mass spectra, **7** exhibited the parent ion peak (M^+), whereas **8** and **9** exhibited intense fragment ion peaks ($[M - nPF_6]^{n+}$; $n = 1$ and 2, respectively). The ^{1}H NMR spectral features of **7** and **9** will be discussed in the following section. Electron paramagnetic resonance (EPR) spectroscopy of **8** showed a signal at $g = 1.9955$, although hyperfine structure was not clearly observed (Figure S1). All attempts to grow single crystals of the TriAAOP derivatives were unsuccessful. Therefore, we carried out density functional theory (DFT) calculations on their model compounds, **7-m**, **8-m**, and **9-m**, in which the *meso*-substituents were replaced with phenyl groups (Figure 1). For the optimized structures, the bond lengths between the *meso*-nitrogen/oxygen and adjacent α-carbon atoms gradually decreased from **7-m** (1.394/1.358 Å) to **8-m** (1.381/1.347 Å) to **9-m** (1.366/1.336 Å), indicating that the oxidation of the 15-aza-5-oxaporphyrin (AOP) ring strengthened the resonance interactions between the p-orbitals of the *meso*-heteroatoms and α-carbon atoms. With this oxidation-induced X–C bond shortening (X = O, N) at the periphery, the porphyrin core is contracted to provide a narrower coordination environment for the central metal in the order **7-m** > **8-m** > **9-m**, as represented by their Zn–N bond lengths of 2.021/2.029 Å for **7-m**, 2.010/2.021 Å for **8-m**, and 2.008/2.013 Å for **9-m**.

2.2 | Aromaticity

The NMR data for **7** and **9** presented below were collected from their freshly prepared samples. The ^{1}H NMR spectrum of **7** in CD_2Cl_2 displayed peaks from the β-pyrrolic, *ortho*-methyl, and *para*-methyl protons at δ 3.8-4.9 (total 8H), 2.30, and 2.17 ppm, respectively, whereas that of **9** in CD_2Cl_2 showed the corresponding protons at δ 7.98-8.66 (total 8H), 2.56, and 1.92 ppm, respectively (Figure 2). The chemical shifts of the β-pyrrolic as well as *ortho*/*para*-methyl protons of **7** basically reflect the paratropic ring-current effect arising from the 20π-electron antiaromatic conjugation and are considerably shifted downfield compared with those of **P0** (δ 3.02 and 4.07 ppm in C_6D_6).[24]

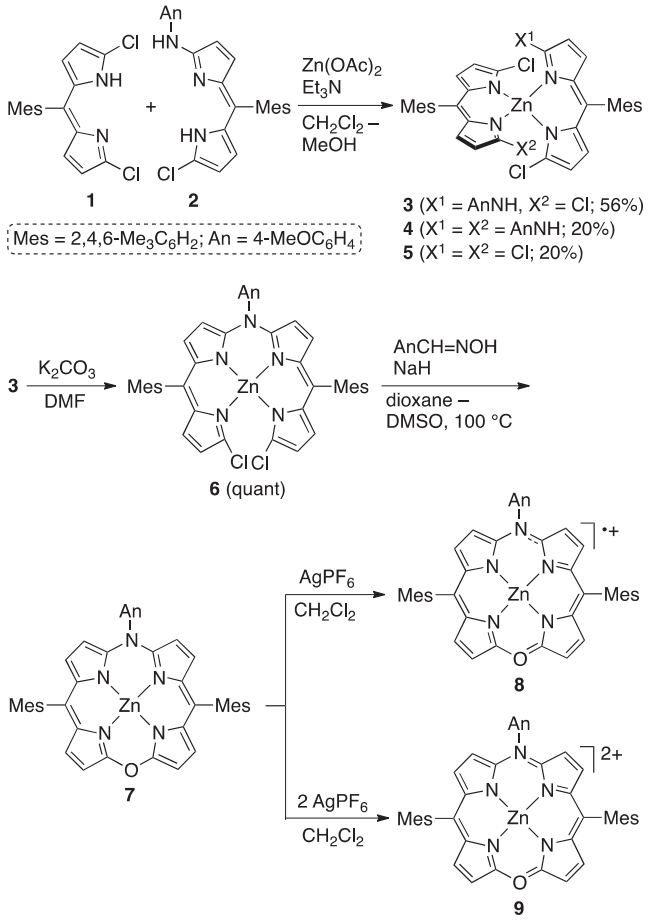

SCHEME 2 Synthesis of **7**, **8**, and **9**

This suggests that the 20π-electron circuit of **7** is less antiaromatic in character than that of **P0**. A similar trend was observed in the ^{1}H NMR spectra of the nickel(II) complexes of DOP and 20π TADAP, where the former *meso*-modified heteroporphyrin exhibited a smaller paratropic ring-current effect than the latter. Probably, the greater electronegativity of oxygen than that of nitrogen hampers global delocalization of its lone-pair electrons in both DOP and 20π TriAAOP. In contrast, the diatropic ring-current effect on the β-pyrrolic protons of **9** was slightly weaker than that of **P2** (δ 8.20 and 8.54 ppm in $CDCl_3$).[24] It appears that the 18π-electron circuit of **9** was less aromatic in character than that of **P2**, although deshielding caused by the inductive effect through the heteroatom-carbon σ bonds should also be considered.

To obtain more insight into the ring-current effects, we calculated nucleus-independent chemical shift (NICS) values[32] at five positions in the π-planes of **7-m** and **9-m** (Figure 1). The NICS(0) values at the midpoints between the two adjacent pyrrole rings (*a*, *b*, and *c*) in **7-m** were +5.79, +7.11, and +6.11 ppm, respectively, indicating that there are global paratropic ring currents in its 20π circuit. In contrast, the NICS(0) values at the corresponding positions in **9-m** were −12.30, −12.31, and −13.42 ppm, respectively, which are apparently affected by diatropic ring currents arising from the 18π circuit. The absolute NICS(0) values calculated for **7-m** and **9-m** are smaller than those calculated for the corresponding models of 20π TADAP **P0-m** (+8.13 and +9.32 ppm for *a* and *b*, respectively) and 18π TADAP **P2-m** (−17.72 and −17.11 ppm for *a* and *b*, respectively).[24] Based on these results, it can be safely concluded that 20π (18π) TriAAOP exhibited weaker antiaromatic (aromatic) character than that of 20π (18π) TADAP in terms of ring-current effects. In both **7-m** and **9-m**, the negative NICS(0) values (from −6.14 to −8.27 ppm) at positions *d* and *e* imply that the pyrrole rings have local diatropic ring currents. The NICS(0) values of **9-m** are less negative than those of a model for the zinc(II) complex of 10,20-dimesityl-5,15-diazaporphyrin (DAP) (−18.93 and −19.22 ppm at the corresponding positions).[33] This indicates that the macrocyclic ring-current effect of 18π TriAAOP is also weaker than that of 18π DAP.

2.3 | Optical and redox properties

The optical properties of the three oxidation states of TriAAOP were investigated by UV-vis-NIR absorption spectroscopy. Table 1 summarizes the experimentally observed data for the TriAAOP, TADAP, and porphyrin/DAP reference materials, and Figure 3A shows the UV-vis-NIR absorption spectra of **7**, **8**, and **9** in CH_2Cl_2. The 20π TriAAOP **7** exhibited two intense absorption bands with absorption maxima (λ_{max}) of 437 and 488 nm, which are blue-shifted compared with those of **P0** (λ_{max} = 444 and 519 nm).[24] In contrast, the lowest-energy band of the 19π TriAAOP **8** (λ_{max} = 1034 nm) was red-shifted compared with that of **P1** (λ_{max} = 890 nm). In addition, an intense band was observed for 18π TriAAOP **9** (λ_{max} = 671 nm) at much longer wavelength than those of the related 18π derivatives, **P2** (λ_{max} = 634 nm)[24] and zinc(II) complexes of DAP (λ_{max} = 584 nm)[33] and 5,10,15-triphenylporphyrin (λ_{max} = 543 nm).[34] It is now evident that the concurrent replacement of two *meso*-methine units of a porphyrin ring with both a nitrene unit (arylimino group) and oxygen atom as well as the addition of positive charge(s) effectively lowered the excitation energies for the generation of the lowest excited states of the 19π and 18π porphyrins.

The successive and quantitative formation of the 19π radical cation and 18π dication was monitored by spectrometric titration; the stepwise addition of tris(4-bromophenyl)ammoniumyl hexachloroantimonate (magic blue) to a CH_2Cl_2 solution of **7** (yellow) revealed continuous spectral changes to **8*** (smoky yellow; 19π radical cation, λ_{max} = 1043 nm) and then to **9*** (green; 18π dication, λ_{max} = 673 nm) with several isosbestic points (Figure 3B).

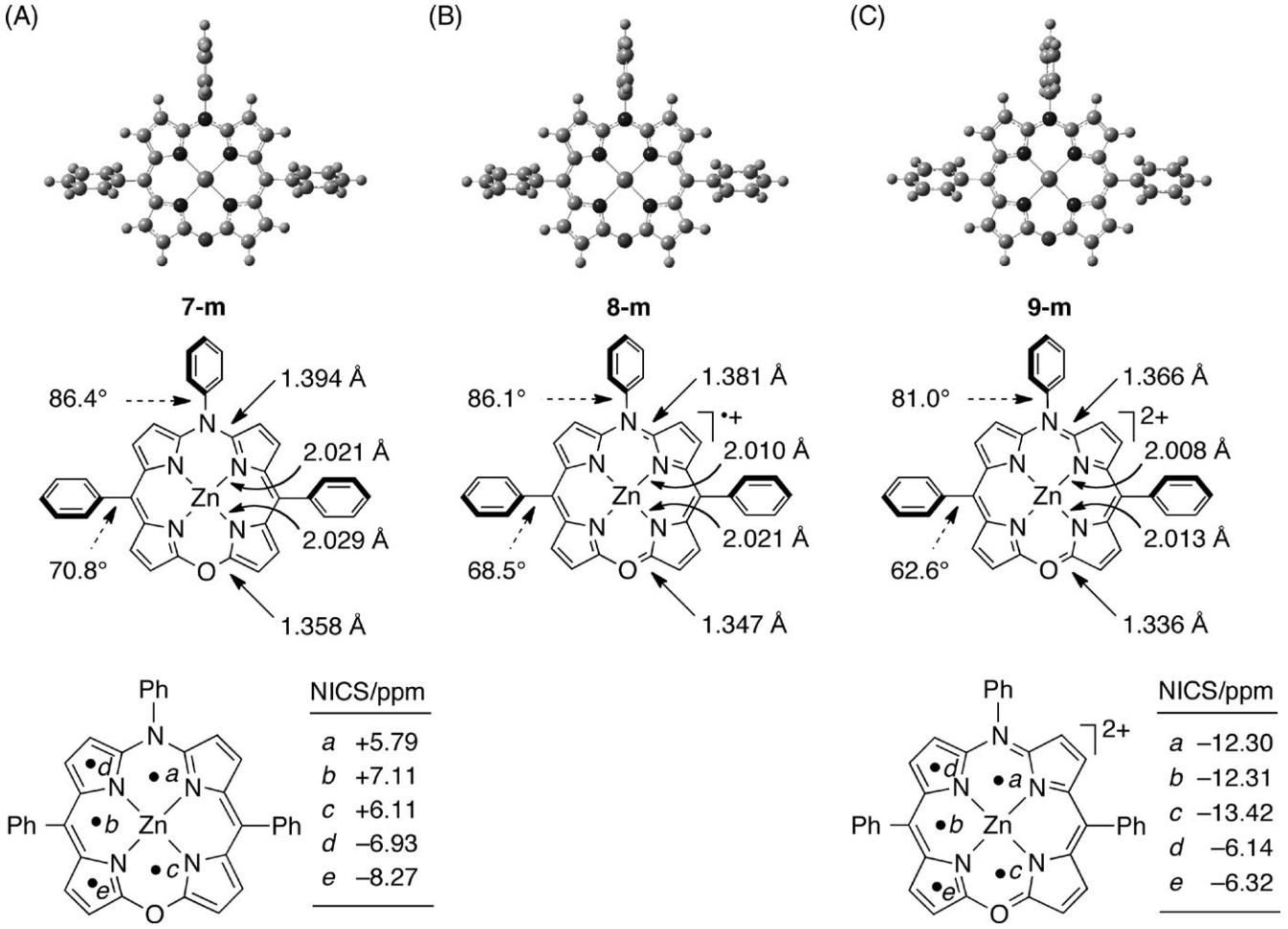

FIGURE 1 Optimized structures, selected bond lengths, dihedral angles, and NICS(0) values calculated by the DFT method with the solvent effect (B3LYP/6-311G(d,p) and Wachters-Hay(f) with PCM, CH_2Cl_2): A, **7-m**, B, **8-m**, C, **9-m**. NICS(0) values at the five positions (*a*-*e*) were calculated at HF-GIAO/6-31G+(d) level

This result strongly supported that the single electron transfer from the TriAAOP π-system to the oxidant occurred stepwise and quantitatively.

To understand the origin of the π–π* electronic transitions of the TriAAOP π-systems, we carried out time-dependent DFT (TD-DFT) calculations on **7-m**, **8-m**, and **9-m** using the B3LYP functional (for the results of **P0-m** and **P2-m**, see ref.[24]). Selected Kohn-Sham orbitals of **7-m**, **9-m**, **P0-m**, and **P2-m** are depicted in Figure 4. The orbital features of the HOMO of **7-m** largely correspond to those of the lowest unoccupied molecular orbital (LUMO) of **9-m**, implying that the two electrons in the HOMO of **7** were removed in the chemical oxidation process to form **9**.

As summarized in Table 2, the lowest-energy excitation for **7-m** was the symmetry-forbidden HOMO-to-LUMO electronic transition, which was not clearly observed in the spectrum of **7**. The intense bands observed for **7** were assigned to combinations of the HOMO−1-to-LUMO and HOMO-to-LUMO+1 electronic transitions (states 2 and 3 for **7-m** in Table 2). In contrast, the lowest-energy band observed for **9** was attributed to the symmetry-allowed HOMO-to-LUMO electronic transition (state 1 for **9-m** in Table 2). The highly electronegative oxygen atom at the *meso* position in the 18π AOP ring (**9-m**) energetically stabilized the LUMO more efficiently than the HOMO relative to the corresponding orbitals of the 18π TADAP ring (**P2-m**) because their LUMOs have moderate orbital coefficients at the *meso*-heteroatoms. This readily explains the red-shifted HOMO-to-LUMO excitation of **9** (λ_{max} = 671 nm) relative to that of **P2** (λ_{max} = 634 nm). The lowest-energy excitation calculated for **8-m** was the HOMO−1-to-SOMO electronic transition, although the calculated excitation energy did not match well with the observed value.

The redox potentials of **7** were measured in CH_2Cl_2 by using cyclic voltammetry with tetrabutylammonium hexafluorophosphate (Bu_4NPF_6) as a supporting electrolyte. As shown in Figure 5, TriAAOP exhibited two separate and reversible redox processes at −0.35 and +0.28 V (vs ferrocene/ferrocenium; Fc/Fc^+), which were attributed to

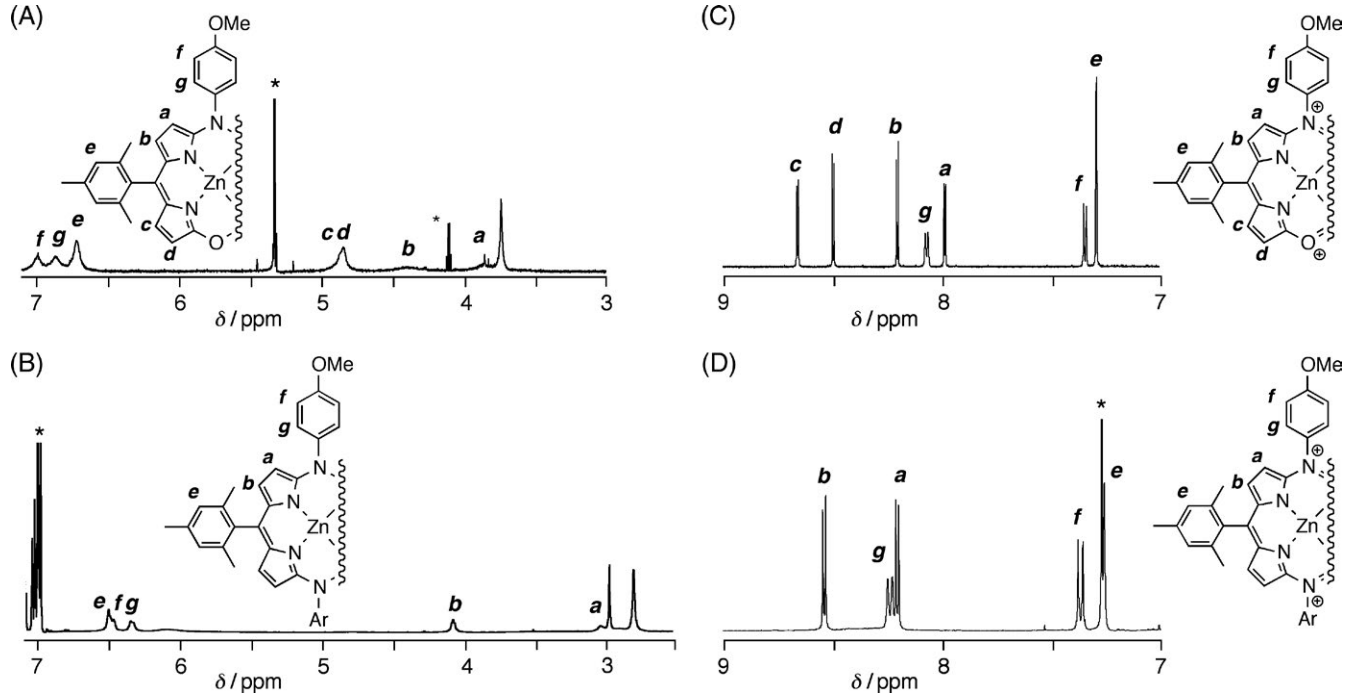

FIGURE 2 ^{1}H NMR spectra of A, **7** in CD_2Cl_2, B, **P0** in C_6D_6, C, **9** in CD_2Cl_2, and D, **P2** in $CDCl_3$. Asterisks indicate residual solvent peaks. 700 MHz for **7** and **9**; 400 MHz for **P0** and **P2**

20π/19π and 19π/18π redox processes, respectively. The redox potentials of TriAAOP were considerably shifted to the positive side ($\Delta E = 0.34$-0.36 V), compared with the corresponding potentials of TADAP. The observed results are in good accordance with the theoretically calculated results for their models (Figure 4); the HOMO of **7-m** ($E = -4.56$ eV) and LUMO of **9-m** ($E = -5.49$ eV) are energetically stabilized compared with the corresponding orbitals of **P0-m** ($E = -4.26$ eV) and **P2-m** ($E = -5.16$ eV), respectively, at the same level of theory.[25] These molecular orbitals have relatively large orbital coefficients at the *meso*-heteroatoms (vide supra) and therefore are markedly stabilized upon introducing the highly electronegative oxygen atom.

TABLE 1 Optical data for **7, 8, 9,** and related zinc(II)–porphyrin derivatives[a]

Compounds	λ_{max}/nm
7	437, 488
8	363, 424, 886, 977, 1034
9	381, 671
P0	444, 519[b]
P1	384, 448, 890[b]
P2	389, 634[b]
ZnDAP	394, 552, 584[c]
ZnPor	418, 543[d]

[a]Measured in CH_2Cl_2 unless otherwise noted.
[b]Data from ref.[23]
[c]ZnDAP = 10,20-dimesityl-5,15-diazaporphyrinatozinc(II), measured in CH_2Cl_2–MeOH; data from ref.[33]
[d]ZnPor = 5,10,15-triphenylporphyrinatozinc(II), measured in toluene; data from ref.[34]

3 | CONCLUSION

We prepared TriAAOPs using metal-templated annulation and redox reactions. The magnetic criteria of aromaticity for the 20π and 18π TriAAOP derivatives were evaluated by NMR spectroscopy and NICS calculations, which revealed that the replacement of the *meso*-methine units with a nitrene unit and oxygen atom decreased both the paratropic and diatropic ring-current effects arising from the porphyrin π-circuits. In addition, the optical and redox properties of TriAAOP were studied using UV-vis-NIR absorption spectroscopy, cyclic voltammetry, and DFT calculations. The *meso*-modification energetically stabilized specific molecular orbitals and, as a result, decreased the electronic excitation energies generating the lowest excited states of the 18π and 19π porphyrins. The observed results were rationally explained by considering the combined effect of the nitrene unit and oxygen atom, which was not observed for the related TADAP and DOP derivatives. The present results highlight the potential of *meso*-heteroatom-modified porphyrins as redox-switchable catalysts and sensitizers; such applications will be studied in due course.

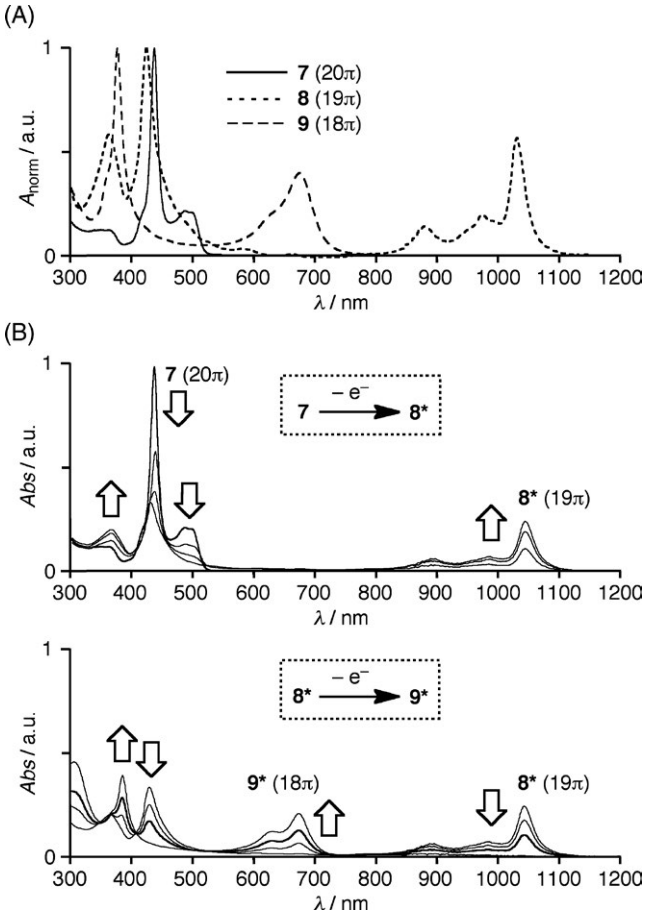

FIGURE 3 A, Normalized UV-vis-NIR absorption spectra of **7** (solid line), **8** (dotted line), and **9** (dashed line) in CH_2Cl_2. B, Spectral changes during the stepwise addition of Magic blue to a CH_2Cl_2 solution of **7** (ca. 1×10^{-5} M); the first oxidation from **7** to **8*** (upper), and the second oxidation from **8*** to **9*** (lower). The counter anion of **8*** and **9*** was hexachloroantimonate

4 | EXPERIMENTAL

NMR spectra were recorded on 700 MHz (Agilent) and/or 400 MHz (Agilent or JEOL JNM-ECP) spectrometers. The ^{1}H chemical shifts are reported in ppm as relative values vs tetramethylsilane. High-resolution mass (HRMS) spectra were measured on a Thermo Fisher Scientific EXACTIVE spectrometer (electron spray–quadrupole). UV-Vis-NIR absorption spectra were measured on a JASCO V-530 spectrometer. UV-vis fluorescence spectrum and quantum yield of **6** were measured on a JASCO FP-8300 spectrometer and a Hamamatsu Photonics Quantaurus-QY spectrometer, respectively. Thin-layer chromatography was performed with Kieselgel 60 F254, and preparative column chromatography was performed using Silica Gel 60 spherical, neutrality. All reactions were performed under an argon or nitrogen atmosphere unless otherwise noted. Compounds **1**[31] and **2**[23,24] were prepared according to the reported procedures.

4.1 | Compounds 3 and 4

A mixture of **1** (455.0 mg, 1.374 mmol), **2** (577.2 mg, 1.384 mmol), $Zn(OAc)_2$ (303.6 mg, 1.654 mmol), triethylamine (1 mL), CH_2Cl_2 (50 mL), and MeOH (50 mL) was stirred for 18 hours at room temperature. The mixture was concentrated under reduced pressure. The residue was then subjected to silica-gel column chromatography (hexane/AcOEt = 10/1). TLC indicated three fractions ($R_f = 0.57$, 0.72, 0.74; hexane/AcOEt = 5/1), of which the second fraction ($R_f = 0.72$) was collected, concentrated, and recrystallized from MeOH to give **3** as a reddish brown solid (622.4 mg, 56%). The other fractions were also collected and recrystallized. The first ($R_f = 0.74$) and third ($R_f = 0.57$) fractions were evaporated to give **4** (201.1 mg, 20%, orange solid) and **5** (128 mg, 20%, reddish brown solid), respectively. Compound **5** was characterized based on the reported spectral data.[24]

3: R_f (hexane/AcOEt = 5/1) = 0.72. Mp 163-164°C ^{1}H NMR (400 MHz, $CDCl_3$): δ 1.95 (s, 3H, *para*-Me), 2.14 (s, 3H, *para*-Me), 2.17 (s, 6H, *ortho*-Me), 2.36 (s, 3H, *ortho*-Me), 2.37 (s, 3H, *ortho*-Me), 3.77 (s, 3H, OMe), 6.08 (d, 1H, $J = 3.8$ Hz, pyrrole-β), 6.16 (d, 1H, $J = 3.8$ Hz, pyrrole-β), 6.19 (d, 1H, $J = 4.4$ Hz, pyrrole-β), 6.30 (d, 1H, $J = 4.4$ Hz, pyrrole-β), 6.31 (s, 1H, NH), 6.57 (d, 1H, $J = 4.4$ Hz, pyrrole-β), 6.59 (d, 1H, $J = 4.4$ Hz, pyrrole-β), 6.76-6.85 (m, 4H, Ar), 6.88 (s, 1H, *meta*-Mes), 6.93 (s, 2H, *meta*-Mes), 6.94 (s, 1H, *meta*-Mes); ^{13}C NMR (100 MHz, $CDCl_3$): δ 19.52, 19.56, 21.04, 21.07, 55.28, 109.82, 110.04, 114.43, 116.59, 122.96, 124.03, 127.52, 127.57, 127.87, 131.92, 132.84, 133.06, 134.64, 135.15, 135.58, 136.05, 136.26, 136.74, 136.77, 136.93, 137.20, 137.28, 137.94, 137.70, 145.52, 147.15, 156.45, 161.98; HRMS (ESI): *m/z* calcd for $C_{43}H_{38}Cl_3N_5OZn$: 810.1428; found: 810.1393 ($[M]^+$).

4: R_f (hexane/AcOEt = 5/1) = 0.74. Mp > 300°C; ^{1}H NMR (400 MHz, $CDCl_3$): δ 2.14 (s, 12H, *ortho*-Me), 2.38 (s, 6H, *para*-Me), 6.24 (d, 4H, $J = 4.0$ Hz, pyrrole-β), 6.54 (d, 2H, $J = 4.0$ Hz, pyrrole-β), 6.95 (s, 4H, Mes-*meta*); ^{13}C NMR (100 MHz, $CDCl_3$): δ 19.63, 21.14, 115.92, 127.68, 132.58, 133.46, 136.82, 137.50, 137.60, 145.73, 146.14; HRMS (ESI): *m/z* calcd for $C_{36}H_{30}Cl_4N_4Zn$: 722.0511; found: 722.0511 ($[M]^+$).

4.2 | Compound 6

A mixture of **5** (621 mg, 0.764 mmol), K_2CO_3 (876 mg, 6.34 mmol), and DMF (40 mL) was stirred for 1 hour at 110°C. After being quenched with water, the aqueous layer was extracted with toluene, and the combined organic extracts were washed with brine, dried over Na_2SO_4, and evaporated under reduced pressure. The residue was then subjected to silica-gel column chromatography (hexane/AcOEt = 10/1). The green fraction ($R_f = 0.44$; hexane/AcOEt = 5/1) was

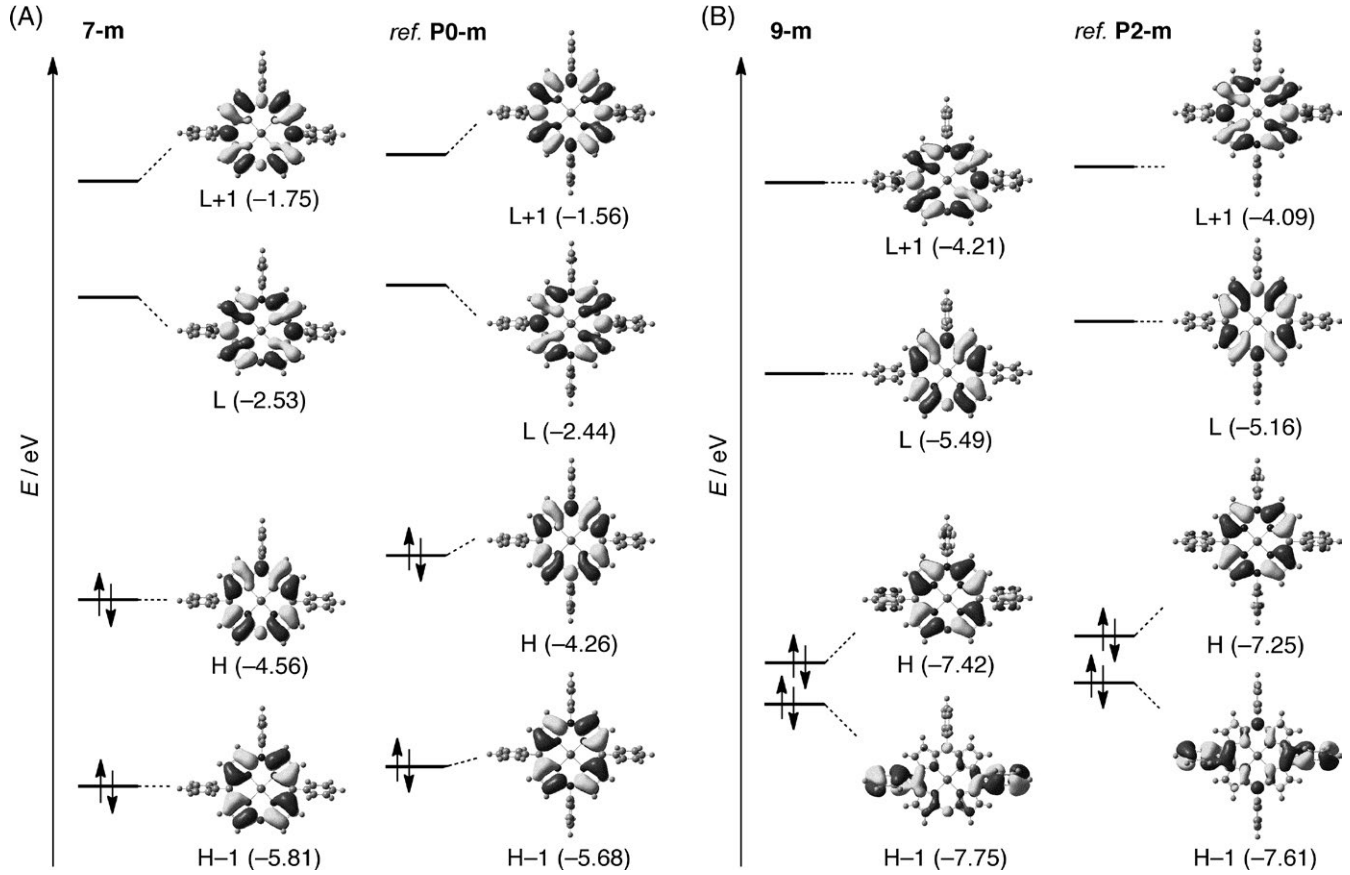

FIGURE 4 Selected Kohn-Sham orbitals and their energies (in eV) of A, **7-m** and **P0-m** and B, **9-m** and **P2-m** calculated by the DFT method with the solvent effect (B3LYP/6-311G(d,p) and Wachters-Hay(f) with PCM, CH_2Cl_2). H = HOMO; L = LUMO. Data for **P0-m** and **P2-m** are taken from ref.[24]

collected and evaporated to give **6** as a green solid (622 mg, quant). Mp 210-213°C; ^{1}H NMR (400 MHz, $CDCl_3$): δ 2.11 (s, 6H, *ortho*-Mes), 2.20 (s, 6H, *ortho*-Mes), 2.36 (s, 6H, *para*-Mes), 3.89 (s, 3H, OMe), 5.61 (d, 2H, $J = 4.4$ Hz, pyrrole-β), 6.32 (d, 2H, $J = 3.8$ Hz, pyrrole-β), 6.33 (d, 2H, $J = 3.8$ Hz, pyrrole-β), 6.53 (d, 2H, $J = 4.4$ Hz, pyrrole-β), 6.93 (s, 4H, Mes-*meta*), 7.02-7.07 (m, 2H, Ar), 7.36-7.41 (m, 2H, Ar); ^{13}C NMR (100 MHz, $CDCl_3$): δ 19.58, 19.78, 21.08, 55.44, 112.25, 114.13, 115.06, 125.19, 126.77, 127.57, 127.59, 130.16, 132.43, 133.32, 133.96, 136.90, 137.06, 137.30, 138.30, 138.59, 139.33, 140.37, 158.01, 159.85; HRMS (ESI): *m/z* calcd for $C_{43}H_{37}Cl_2N_5OZn$: 773.1661, found: 773.1663 [M^+]; UV/Vis (CH_2Cl_2): λ_{max} (log ε) 452 (4.89), 669 (3.90) nm. In CH_2Cl_2, **6** emitted fluorescence ($\lambda_{ex} = 450$ nm) with the emission maximum at 736 nm, and fluorescence quantum yield was determined to be 1.3%. The UV-vis absorption and fluorescence spectra of **6** are summarized in Figure S1.

4.3 | Compound 7

Sodium hydride (60% dispersion in a mineral oil, 53.6 mg, 1.34 mmol) was added to a mixture of well-dried DMSO (20 mL) and dioxane (20 mL), and the resulting mixture was heated at 70°C for 30 minutes. 4-Methoxybenzaldoxime (317.5 mg, 2.10 mmol) was added, and the mixture was stirred at the same temperature. After 1 hour, **6** (104.7 mg, 0.135 mmol) was added and the resulting mixture was heated at 100°C for 1.5 hour. After being quenched with water, the aqueous layer was extracted with toluene, and the combined organic extracts were dried over Na_2SO_4 and evaporated under reduced pressure. The residue was then subjected to silica-gel column chromatography (hexane/AcOEt = 5/1). The yellow fraction ($R_f = 0.51$; hexane/AcOEt = 5/1) was collected and evaporated to give **7** as a yellow solid (13.2 mg, 14%). ^{1}H NMR (700 MHz, CD_2Cl_2): δ = 2.17 (s, 6H, *para*-Me), 2.30 (s, 12H, *ortho*-Me), 3.73 (s, 3H, OMe), 3.84 (broad-s, 2H, pyrrole-β), 4.38 (broad-s, 2H, pyrrole-β), 4.84 (broad-s, 4H, pyrrole-β), 6.71 (s, 4H, Mes-*meta*), 6.86 (broad-s, 2H, Ar), 6.98 (broad-s, 2H, Ar); HRMS (ESI): *m/z* calcd for $C_{43}H_{37}N_5O_2Zn$: 719.2233, found: 719.2229 ([M^+]); UV/Vis (CH_2Cl_2): λ_{max} = 437, 488 nm.

4.4 | Compound 8

This compound was found to gradually decompose in a concentrated solution and on silica gel. Therefore, we

TABLE 2 Excitation energies and oscillator strengths of **7-m**, **8-m**, and **9-m** calculated by the TD-DFT method[a]

State	Excitation energy (eV)	Excitation energy (nm)	Oscillator strength	Excitation (weight, %)
7-m				
1	1.44	860	0.013	H → L (100.0)
2	2.50	497	0.110	H → L + 1 (71.9), H–1 → L (28.1)
3	3.21	386	1.196	H–1 → L (59.1), H → L + 1 (22.8)
4	3.25	382	0.199	H → L + 2 (83.4)
8-m				
1	1.39	892	0.156	H–1 → S (71.8), S → L (25.4)
2	1.49	831	0.111	S → L (70.8), H–1 → S (25.4)
10	2.63	472	0.062	S → L + 1 (31.5)
19	3.19	389	0.203	H–7 → L (18.4)
9-m				
1	1.81	685	0.029	H → L (95.9)
2	1.87	664	0.346	H → L (69.5), H–4 → L (28.4)
6	2.27	547	0.105	H–5 → L (85.3)
14	3.04	407	0.502	H–1 → L + 1 (94.7)
15	3.14	395	0.137	H-4 → L + 1 (61.6)
18	3.41	364	1.072	H → L + 1 (33.8)

[a]B3LYP/6-311G(d,p) and Wachters-Hay(f) (PCM, CH_2Cl_2) at the optimized structures. H: HOMO; L: LUMO; S: SOMO. Except for the lowest-energy excited states of **7-m** and **9-m**, the states whose oscillator strengths are less than 0.1 are not included.

characterized it in the dissolved state by using UV-vis spectroscopy and HR-ESI mass spectrometry. Silver(I) hexafluorophosphate (4.6 mg, 18 μmol) was added to a CH_2Cl_2 solution (20 mL) of **7** (13 mg, 18 μmol). The resulting solution was passed through a Celite bed, and the filtrate was immediately characterized by the abovementioned methods. HRMS (ESI): *m/z* calcd for $C_{43}H_{37}N_5O_2Zn$: 719.2255, found: 719.2261 $[M - (PF_6)^+]$; UV/Vis (CH_2Cl_2): λ_{max} = 363, 424, 886, 977, 1034 nm.

4.5 | Compound 9

This compound was found to gradually decompose in a concentrated solution. Therefore, we characterized it in the dissolved state by using ^{1}H NMR as well as UV-vis spectroscopy and HR-ESI mass spectrometry. Silver(I) hexafluorophosphate (ca. 2 mg, ca. 8 μmol) was added to a CD_2Cl_2 solution (4 mL) of **7** (ca. 2 mg, ca. 3 μmol). The color of the solution quickly turned to green, and the product was immediately characterized by the abovementioned methods. ^{1}H NMR (700 MHz, CD_2Cl_2): δ = 1.92 (s, 6H, *para*-Me), 2.56 (s, 12H, *ortho*-Me), 4.06 (s, 3H, OMe) 7.29 (s, 4H, Mes-*meta*), 7.34 (d, 2H, *J* = 8.0 Hz, Ar), 7.98 (d, 2H, *J* = 4.9 Hz, pyrrole-β), 8.07 (d, 2H, *J* = 8.0 Hz, Ar), 8.20 (d, 2H, *J* = 4.9 Hz, pyrrole-β), 8.49 (d, 2H, *J* = 4.9 Hz, pyrrole-β), 8.66 (d, 2H, *J* = 4.9 Hz, pyrrole-β); HRMS (ESI): *m/z* calcd for $C_{43}H_{37}N_5OZn$: 359.6114 (*z* = 2), 719.2233 (*z* = 1), found: 359.6110 (*z* = 2), 719.2227 (*z* = 1) $[M - 2(PF_6)^{z+}]$; UV/Vis (CH_2Cl_2): λ_{max} = 381, 671 nm.

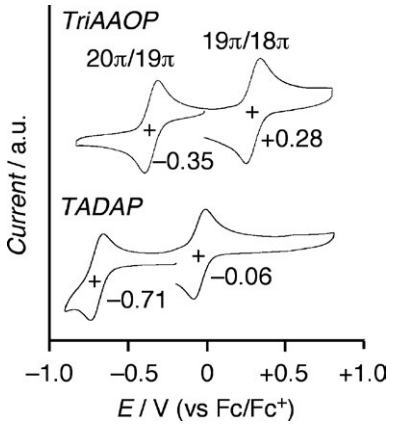

FIGURE 5 Cyclic voltammograms for TriAAOP **7** (upper) and TADAP **P1** (lower) measured in CH_2Cl_2 with Bu_4NPF_6 as the supporting electrolyte: Scan rate = 60 mV/s

4.6 | Electrochemical measurements

Redox potentials of **7** in CH_2Cl_2 were measure by cyclic voltammetry at room temperature on a CH Instruments model 660A electrochemical workstation using a glassy

carbon working electrode, a platinum wire counter electrode, and an Ag/Ag^+ [0.01 M $AgNO_3$, 0.1 M Bu_4NPF_6 (MeCN)] reference electrode. The scan rate was 60 mV/s. The potentials were calibrated to a ferrocene/ferrocenium (Fc/Fc^+) couple.

4.7 | EPR measurements

The EPR spectrum of **8** was measured at room temperature by using a JEOL JES-FA200 spectrometer equipped with an OXFORD ESR900 He-flow cryostat. The sample was prepared as a 0.1 mmol/L solution in CH_2Cl_2. After three freeze-pump-thaw cycles, the solution sample in a quartz tube was sealed by frame. The static magnetic field and microwave frequency were measured by an Echo Electronics EFM-2000 gauss meter and a TakedaRiken TR5212 microwave counter, respectively.

4.8 | Computational details

The geometries of the model compounds were optimized using the DFT method. The basis sets used were 6-311G(d,p) basis set[35] for H, C, and N and the Wachters-Hay all electron basis set[36] supplemented with one f-function (exponent: 1.62) for Zn. The functional of DFT was the Becke, three-parameter, Lee-Yang-Parr (B3LYP) exchange-correlation functional.[37] We confirmed that the optimized geometries were not in saddle but in stable points. The NICS values[32] for **7-m** and **9-m** were calculated at the Hartree-Fock level with gauge-including atomic orbitals (GIAOs) at the DFT-optimized geometries. The basis set used for the NICS calculations was 6-31 + G(d).[38] The excitation energies and oscillator strengths listed in Table 2 were computed with the time-dependent density functional theory (TD-DFT) method.[39] All the calculations were carried out using the Gaussian 09 suite of programs.[40]

ACKNOWLEDGMENTS

This work was supported by JSPS KAKENHI (Grant Number: 18H01961 to YM, 15K05392 and 18K05036 to HN).

ORCID

Yoshihiro Matano https://orcid.org/0000-0003-3377-0004

REFERENCES

[1] a) K. M. Kadish, E. Van Caemelbecke, G. Royal, in The Porphyrin Handbook, Vol *8* (Eds: K. M. Kadish, K. M. Smith, R. Guilard), Academic Press, San Diego, CA **2000**, pp. 1–114; b) B. K. Reddy, A. Basavarajappa, M. D. Ambhore, V. G. Anand, *Chem. Rev.* **2017**, *117*, 3420, and references therein.

[2] M. Pohl, H. Schmickler, J. Lex, E. Vogel, *Angew. Chem. Int. Ed. Engl.* **1991**, *30*, 1693.

[3] J. Setsune, K. Kashihara, K. Wada, H. Shinozaki, *Chem. Lett.* **1999**, *28*, 847.

[4] T. P. Vaid, *J. Am. Chem. Soc.* **2011**, *133*, 15838.

[5] J. S. Reddy, V. G. Anand, *J. Am. Chem. Soc.* **2008**, *130*, 3718.

[6] B. K. Reddy, S. C. Gadekar, V. G. Anand, *J. Am. Chem. Soc.* **2015**, *51*, 8276.

[7] S. P. Panchal, S. C. Gadekar, V. G. Anand, *Angew. Chem. Int. Ed.* **2016**, *55*, 7797.

[8] J. A. Cissell, T. P. Vaid, A. L. Rheingold, *J. Am. Chem. Soc.* **2005**, *127*, 12212.

[9] J. A. Cissell, T. P. Vaid, G. P. A. Yap, *J. Am. Chem. Soc.* **2007**, *129*, 7841.

[10] J. A. Cissell, T. P. Vaid, A. G. DiPasquale, A. L. Rheingold, *Inorg. Chem.* **2007**, *46*, 7713.

[11] E. W. Y. Wong, C. J. Walsby, T. Storr, D. B. Leznoff, *Inorg. Chem.* **2010**, *49*, 3343.

[12] A. Weiss, M. C. Hodgson, P. D. W. Boyd, W. Siebert, P. J. Brothers, *Chem. Eur. J.* **2007**, *13*, 5982.

[13] P. J. Brothers, *Chem. Commun.* **2008**, *44*, 2090.

[14] C. Liu, D.-M. Shen, Q.-Y. Chen, *J. Am. Chem. Soc.* **2007**, *129*, 5814.

[15] Y. Matano, T. Nakabuchi, S. Fujishige, H. Nakano, H. Imahori, *J. Am. Chem. Soc.* **2008**, *130*, 16446.

[16] Y. Matano, H. Imahori, *Acc. Chem. Res.* **2009**, *42*, 1193.

[17] T. Nakabuchi, M. Nakashima, S. Fujishige, H. Nakano, Y. Matano, H. Imahori, *J. Org. Chem.* **2010**, *75*, 375.

[18] Y. Matano, H. Nakabuchi, H. Imahori, *Pure Appl. Chem.* **2010**, *82*, 583.

[19] T. Yoshida, W. Zhou, T. Furuyama, D. B. Leznoff, N. Kobayashi, *J. Am. Chem. Soc.* **2015**, *137*, 9258.

[20] T. Syzuki, H. Kotani, T. Ishizuka, Y. Shiota, K. Yoshizawa, T. Kojima, *Angew. Chem. Int. Ed.* **2018**, *57*, 1973.

[21] A. Yamaji, H. Tsurugi, Y. Miyake, K. Mashima, H. Shinokubo, *Chem. Eur. J.* **2016**, *22*, 3956.

[22] T. Sugai, M. Minoura, H. Nakano, Y. Matano, *Bull. Chem. Soc. Jpn.* **2018**, *91*, 1264.

[23] T. Satoh, M. Minoura, H. Nakano, K. Furukawa, Y. Matano, *Angew. Chem. Int. Ed.* **2016**, *55*, 2235.

[24] K. Sudoh, T. Satoh, T. Amaya, K. Furukawa, M. Minoura, H. Nakano, Y. Matano, *Chem. Eur. J.* **2017**, *23*, 16364.

[25] K. Sudoh, T. Hatakeyama, K. Furukawa, H. Nakano, Y. Matano, *J. Porphyrins Phthalocyanines* **2017**, *22*, 542.

[26] Y. Matano, *Chem. Rev.* **2017**, *117*, 3138.

[27] M. J. Broadhurst, R. Grigg, A. W. Johnson, *J. Chem. Soc. Perkin Trans.* **1972**, *1*, 1124.

[28] A. Nishiyama, M. Fukuda, S. Mori, K. Furukawa, H. Fliegl, H. Furuta, S. Shimizu, *Angew. Chem. Int. Ed.* **2018**, *57*, 9728.

[29] H. Kamiya, T. Kondo, T. Sakida, S. Yamaguchi, H. Shinokubo, *Chem. Eur. J.* **2012**, *18*, 16129.

[30] N. Wachi, T. Kondo, S. Ito, S. Hiroto, J.-Y. Shin, H. Shinokubo, *J. Porphyrins Phthalocyanines* **2014**, *18*, 675.

[31] T. Sakida, S. Yamaguchi, H. Shinokubo, *Angew. Chem. Int. Ed.* **2011**, *50*, 2280.

[32] P. R. von Schleyer, C. Maerker, A. Dransfeld, H. Jiao, N. J. R. van Eikema Hommes, *J. Am. Chem. Soc.* **1996**, *118*, 6317.

[33] Y. Matano, T. Shibano, H. Nakano, Y. Kimura, H. Imahori, *Inorg. Chem.* **2012**, *51*, 12879.
[34] K. Tomizaki, A. B. Lysenko, M. Taniguchi, J. S. Lindsey, *Tetrahedron* **2004**, *60*, 2011.
[35] R. Krishnan, J. S. Binkley, R. Seeger, J. A. Pople, *J. Chem. Phys.* **1980**, *72*, 650.
[36] a) A. J. H. Wachters, *J. Chem. Phys.* **1970**, *52*, 1033; b) P. J. Hay, *J. Chem. Phys.* **1977**, *66*, 4377; c) K. Raghavachari, G. W. Trucks, *J. Chem. Phys.* **1989**, *91*, 1062.
[37] a) A. D. Becke, *J. Chem. Phys.* **1993**, *98*, 5648; b) C. Lee, W. Yang, R. G. Parr, *Phys. Rev. B* **1988**, *37*, 785.
[38] a) W. J. Hehre, R. Ditchfield, J. A. Pople, *J. Chem. Phys.* **1972**, *56*, 2257; b) P. C. Hariharan, J. A. Pople, *Theor. Chim. Acta* **1973**, *28*, 213; c) T. Clark, J. Chandrasekhar, G. W. Spitznagel, P. R. von Schleyer, *J. Comput. Chem.* **1983**, *4*, 294; d) V. Rassolov, J. A. Pople, M. Ratner, T. L. Windus, *J. Chem. Phys.* **1998**, *109*, 1223.
[39] E. T. Cancès, B. Mennucci, J. Tomasi, *J. Chem. Phys.* **1997**, *107*, 3032.
[40] M. J. Frisch, G. W. Trucks, H. B. Schlegel, G. E. Scuseria, M. A. Robb, J. R. Cheeseman, G. Scalmani, V. Barone, B. Mennucci, G. A. Petersson, H. Nakatsuji, M. Caricato, X. Li, H. P. Hratchian, A. F. Izmaylov, J. Bloino, G. Zheng, J. L. Sonnenberg, M. Hada, M. Ehara, K. Toyota, R. Fukuda, J. Hasegawa, M. Ishida, T. Nakajima, Y. Honda, O. Kitao, H. Nakai, T. Vreven, J. A. Montgomery Jr., J. E. Peralta, F. Ogliaro, M. Bearpark, J. J. Heyd, E. Brothers, K. N. Kudin, V. N. Staroverov, T. Keith, R. Kobayashi, J. Normand, K. Raghavachari, A. Rendell, J. C. Burant, S. S. Iyengar, J. Tomasi, M. Cossi, N. Rega, J. M. Millam, M. Klene, J. E. Knox, J. B. Cross, V. Bakken, C. Adamo, J. Jaramillo, R. Gomperts, R. E. Stratmann, O. Yazyev, A. J. Austin, R. Cammi, C. Pomelli, J. W. Ochterski, R. L. Martin, K. Morokuma, V. G. Zakrzewski, G. A. Voth, P. Salvador, J. J. Dannenberg, S. Dapprich, A. D. Daniels, Ö. Farkas, J. B. Foresman, J. V. Ortiz, J. Fox, D. J. Cioslowski, Gaussian 09, Revision D.01, Gaussian, Inc., Wallingford CT **2013**.

SUPPORTING INFORMATION

Additional supporting information may be found online in the Supporting Information section at the end of the article.

How to cite this article: Sudoh K, Furukawa K, Nakano H, Shimizu S, Matano Y. Synthesis and properties of redox-switchable zinc complexes of 10,15,20-triaryl-15-aza-5-oxaporphyrin. *Heteroatom Chem*. 2018;29: e21456. https://doi.org/10.1002/hc.21456